Electronic spectroscopy of the alkaline-earth halide cluster Ca_2Cl_3

Julio D. Lobo, Andrei Deev, Chi-Kin Wong, James M. Spotts,[a] and Mitchio Okumura[b]
Arthur Amos Noyes Laboratory of Chemical Physics, California Institute of Technology, Pasadena, California 91125

(Received 6 November 2000; accepted 16 January 2001)

A visible spectrum of the cluster Ca_2Cl_3 was observed from 651 to 630 nm by $1+1'$ resonant multiphoton ionization spectroscopy. Spectra were obtained for each of the four isotopomers: $Ca_2{}^{35}Cl_3$, $Ca_2{}^{35}Cl_2{}^{37}Cl$, $Ca_2{}^{35}Cl{}^{37}Cl_2$, and $Ca_2{}^{37}Cl_3$. The spectra were composed of a strong origin band at 15 350.8 cm^{-1} and several very weak vibronic bands. All of the bands were sharp with partially resolved rotational band contours. Density functional calculations predicted three minimum energy isomers. The spectrum was assigned to the $^2B_2 \leftarrow \tilde{X}\,^2A_1$ transition of the lowest energy isomer, a planar C_{2v} structure having a ring of two Cl and two Ca atoms and a terminal Cl atom. The ring isomer of Ca_2Cl_3 has the unpaired electron localized on one Ca^{2+} ion to form a Ca^+ chromophore. The two other predicted isomers, a D_{3h} trigonal bipyramid and a C_{2v} planar V-shaped structure, were not consistent with the observations. © *2001 American Institute of Physics.* [DOI: 10.1063/1.1353547]

I. INTRODUCTION

Salt clusters are model systems for understanding ionic interactions. Their properties can often be calculated using simple electrostatic interactions to describe the attractive potentials. Alkali halide clusters have received much attention, because they are the simplest of the ionic salts.[1] Clusters as small as 40 atoms are predicted to have cubic structures characteristic of the bulk salt crystal. Smaller clusters however, can have several distinct isomers, including planar square lattice fragments and three-dimensional bridged structures. In contrast, alkaline-earth halide clusters are poorly studied. Bulk $CaCl_2$ salt has a rutilelike structure, in which the Cl atoms form a hexagonal closest packed structure and the Ca atoms fill octahedral holes in alternating rows.[2] The structures of small alkaline-earth halide clusters, as well as their transition to bulklike geometries with increasing size, are not known.

The structures of alkaline-earth dihalides have been the subject of some controversy.[3] Klemperer and colleagues demonstrated the existence of nonzero dipole moments in electric deflection experiments.[4,5] There have since been numerous investigations concerning the factors governing the propensity for linear versus bent geometries.[3,6–8] Polarization and *d*-hybridization appear to play important roles. The ''dimer'' species M_2X_4 have been computed to have many isomers, generally with two or more halogen atoms bridging the metal centers.[6]

Salt clusters with a closed shell ionic framework and outer shell electrons, such as Na_2F are termed excess-electron clusters. These radial clusters are suitable for spectroscopic investigation, because they possess bound-to-bound optical transitions. These transitions have been observed for the alkali halide clusters of composition Na_nF_{n-1}. Theoretical and experimental work on these small alkali halide clusters[9–15] show that, depending on the structure and size of the cluster, the excess electron can be localized in a lattice vacancy, around a sodium atom, or in delocalized surface or bulk states.

The analogous clusters of alkaline-earth halides have not been studied. However, diatomic alkaline-earth halides, which can be treated as an ionic $M^{2+}X^-$ core and an electron, have been investigated for decades.[16–19] Field and coworkers have developed a zero-parameter one electron model based on ligand-field theory that describes the electronic states of these diatomics with semiquantitative accuracy. This picture also forms the basis for the pure precession model[20–23] developed for describing spin–rotation coupling in complexes of alkaline-earth metal atoms with polyatomic ligands. Alternatives include extension of Rittner's polarization model.[24–28] Jungen and co-workers[29] have developed more accurate calculations of Rydberg states using multichannel quantum defect theory, which treats interaction of the electron with the ionic core by scattering methods.

The diatomic CaCl is typical of the alkaline-earth halides. Excited electronic states have been observed from 16 093 cm^{-1} and higher.[30] The electronic states of CaCl arise from Ca^+ free ion states in the field of the Cl^- ligand. The lowest lying transitions of the atomic ion Ca^+ are $(3d_{3/2})^1 \leftarrow (4s_{1/2})^1$ at 13 650.19 cm^{-1}, and $(4p_{1/2})^1 \leftarrow (4s_{1/2})^1$ at 25 191.51 cm^{-1}. The presence of the chloride ion leads to extensive mixing and shifting of the free Ca^+ atomic states. For example, the first excited state of CaCl, the $A\,^2\Pi$ state at 16 093 cm^{-1}, is predominantly $4p$ in character rather than $3d$, but it contains mixtures of other Ca^+ orbitals as well.

Ca_2Cl_3 is the smallest neutral polyatomic alkaline-earth halide that can be modeled as an unpaired electron bound to a framework of closed shell ions, Ca^{+2} and Cl^-. In analogy with small alkali halide clusters, there may be several isomers, which could be linear, planar, and/or bridged. The un-

[a]Present address: Children's Hospital, Department of Neuroscience, Enders Laboratories 260, 300 Longwood Avenue, Boston, Massachusetts 02115.
[b]Author to whom correspondence should be addressed. Electronic mail: mo@its.caltech.edu

paired electron may be localized on one Ca^+, as in CaCl, or it may be shared between the two Ca^{+2} ions. The nature of the charge distribution should influence the energetics of the different isomers. Like CaCl, Ca_2Cl_3 should have transitions in the visible or ultraviolet (UV), which allow direct spectroscopic detection.

In this paper we present an optical spectrum of the alkaline-earth halide cluster Ca_2Cl_3 detected by resonance enhanced multiphoton ionization (REMPI) spectroscopy. Quantum chemistry calculations using density functional theory (DFT) are used to locate minimum energy isomers and to determine their energies, vibrational frequencies, and excited states. By comparing the observed spectrum to the predicted properties, we can unambiguously assign the spectrum.

II. EXPERIMENT

The experimental apparatus will only be briefly described. Details have been published elsewhere.[31] Ca_2Cl_3 was produced by laser ablation of calcium metal in a supersonic molecular expansion of a CCl_4/Ar mixture. The neutral molecules were formed in the ablation plasma, expanded into vacuum, and skimmed into a second region to form a molecular beam. Subsequently, the molecules were resonantly excited and then ionized by simultaneous pulses from two lasers in a $1+1'$ REMPI process. Ionization occurred in the extraction region of a time-of-flight (TOF) mass spectrometer. The ions were separated in time and collected on a microchannel plate detector. The spectra were obtained by scanning the excitation photon frequency while integrating the desired mass peak.

The CCl_4 (Aldrich, 99+%) was entrained in argon carrier gas by placing a bubbler filled with room temperature CCl_4 liquid on the gas line. The pressure in the gas line was 9.3 bar. The gas was pulsed into the source vacuum chamber by a piezo-electric driven valve at 19 Hz in 180 μs long pulses. After the valve seal, the gas traveled through a 13 mm channel. The calcium rod was placed immediately at the exit of the channel (see Fig. 1). The calcium rods were machined from 99.8% pure ingots of calcium (Alfa Aesar). The rod was ablated by 25 mJ pulses of 1.064 μm light from a Nd:YAG (Continuum: Surelight I) laser focused to a 0.5 mm diameter spot. The rod was spun at 1 rpm and translated vertically.

The gas pulse expanded into a vacuum chamber held at an average pressure of 8×10^{-5} Torr (base pressure 2×10^{-7} Torr). The jet was then skimmed 7.5 cm from the nozzle to form a molecular beam in a second vacuum region kept at 1.5×10^{-6} Torr. The rotational temperature of diatomic CaCl produced under these conditions was typically 7–10 K. The molecular beam was crossed by the laser beams 20.3 cm from the tip of the skimmer.

The excitation step was performed by visible radiation from a Nd:YAG (Continuum NY61-20) pumped tunable dye laser (Continuum TDL51). DCM dye was used to generate photons in the 15 110 to 16 000 cm^{-1} range. The dye laser beam was slightly focused to a 5 mm diameter spot. The linewidth of the dye laser was 0.1 cm^{-1}. Observed band intensities varied over four orders of magnitude. A wide range of fluences were needed to prevent saturation. Pulse energies were varied from 1 μJ to 10 mJ with neutral density filters as needed. When recording unsaturated spectra, the power dependence of each band was first measured to determine the saturation limit. The bands were then scanned in the linear regime.

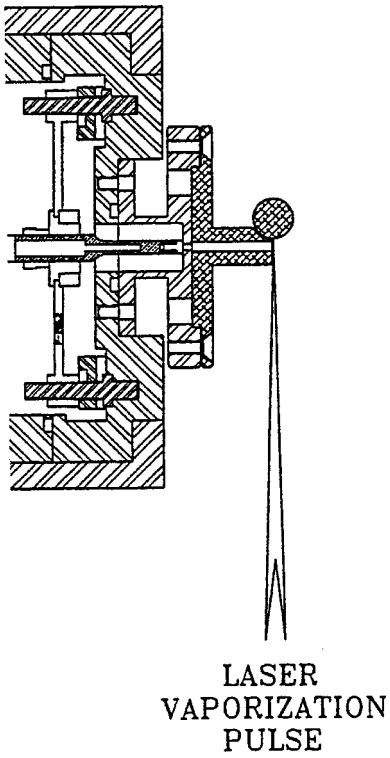

FIG. 1. Laser vaporization source. The calcium rod was ablated at the throat of a supersonic expansion of a CCl_4/Ar mixture.

An excimer laser (Lamda Physik EMG101) was used for the ionization step. The 308 nm, 20 ns pulses were focused into a 2×4 mm rectangular spot, overlapping with the dye laser beam. The ionization took place in the extraction region of a Wiley–McLaren TOF mass spectrometer. The ions were accelerated to an energy of 3 keV, mass separated in a 1.0 m TOF tube, and detected by dual Chevron microchannel plates (Galileo Electro-Optics/Burle FTD-2003). The signal was amplified by a Comlinear CLC 401 amplifier. Mass spectra were recorded with a LeCroy 8818A transient digitizer. To collect an optical spectrum, ion signal of the selected mass peak was integrated (SRS 250 Gated Integrator), digitized (Keithley Metrabyte DAS1602 Acquisition board), and recorded as a function of dye laser frequency.

III. EXPERIMENTAL RESULTS

A. TOF mass spectrum

Figure 2 displays a typical TOF mass spectrum. The most prominent features in the spectrum are Ca^+ and $CaCl^+$ ion peaks. CaO^+ and $CaOH^+$ also appear in the spectrum as minor features. Four peaks are observed for $Ca_2Cl_3^+$, as can be seen in the inset in Fig. 2. $Ca_2Cl_3^+$ peaks are observed only when the excitation photon is in resonance with a Ca_2Cl_3

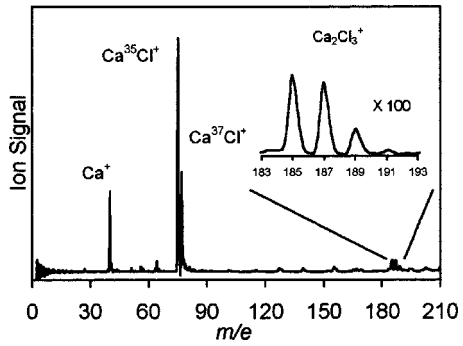

FIG. 2. Multiphoton time-of-flight (TOF) mass spectrum. Spectrum was recorded by ionizing with 651.2 nm and 308 nm radiation. Inset: Ca_2Cl_3 isotopomer peaks. Relative intensities of the Ca_2Cl_3 peaks are close to those expected from the natural chlorine isotope abundances.

transition, while Ca^+ and $CaCl^+$ peaks are observed even without resonant excitation. The spectrum shown in Fig. 2 is obtained when the excitation laser is tuned to the Ca_2Cl_3 0–0 transition at 15 350.8 cm^{-1}. The intensity of $Ca_2Cl_3^+$ is approximately 0.07 relative to the $CaCl^+$ intensity at this frequency.

The four mass peaks of $Ca_2Cl_3^+$ are assigned to the four possible combinations of the chlorine isotopes: $Ca_2{}^{35}Cl_3$ (185 amu), $Ca_2{}^{35}Cl_2{}^{37}Cl$ (187 amu), $Ca_2{}^{35}Cl{}^{37}Cl_2$ (189 amu), and $Ca_2{}^{37}Cl_3$ (191 amu). The observed intensity ratio of the peaks, 1:0.84:0.31:0.039, agrees well with that predicted by the natural isotope abundance, 1:0.96:0.31:0.033.

B. REMPI spectra of Ca_2Cl_3

Visible $1+1'$ REMPI spectra were obtained for each of the four isotopomers of Ca_2Cl_3 in the range from 15 110 to 16 000 cm^{-1}. Unsaturated scans of $Ca_2{}^{35}Cl_3$ and $Ca_2{}^{35}Cl_2{}^{37}Cl$ were acquired with 0.12 cm^{-1} step size. The signals of $Ca_2{}^{35}Cl{}^{37}Cl_2$ and $Ca_2{}^{37}Cl_3$ were near the detection noise limit when unsaturated. We therefore scanned these spectra under saturating conditions (35 mJ/cm^2) and a typical step size of 0.6 cm^{-1} to locate the band frequencies.

The overall spectra of the four isotopomers are similar, but differ in detail. A REMPI spectrum of $Ca_2{}^{35}Cl_3$ is shown in Fig. 3(a). Three of the bands are shown in detail in Figs. 4(a), 4(b), and 4(c). All spectra are dominated by a single intense band with center at $15\,350.8 \pm 0.2\ cm^{-1}$ and a series of significantly weaker vibronic bands up to 640 cm^{-1} to the blue. The bands of the higher-mass isotopomers are slightly redshifted (0.0 to 6.8 cm^{-1}), with the magnitude of the redshift increasing with increasing frequency and mass. For $Ca_2{}^{35}Cl_2{}^{37}Cl$ and $Ca_2{}^{35}Cl{}^{37}Cl_2$, several of the observed bands are also split.

There are no extended progressions; however, the spectrum repeats itself. The second strongest band at 15 616.7 cm^{-1}, is the origin for a set of approximately nine bands with a spectral frequency pattern that is nearly identical to the main bands observed in the first 270 cm^{-1}. The relative intensities are roughly similar as well. The last band in the sequence, at 15 881 cm^{-1}, may be an overtone of the mode giving rise to the 15 616.7 cm^{-1} band.

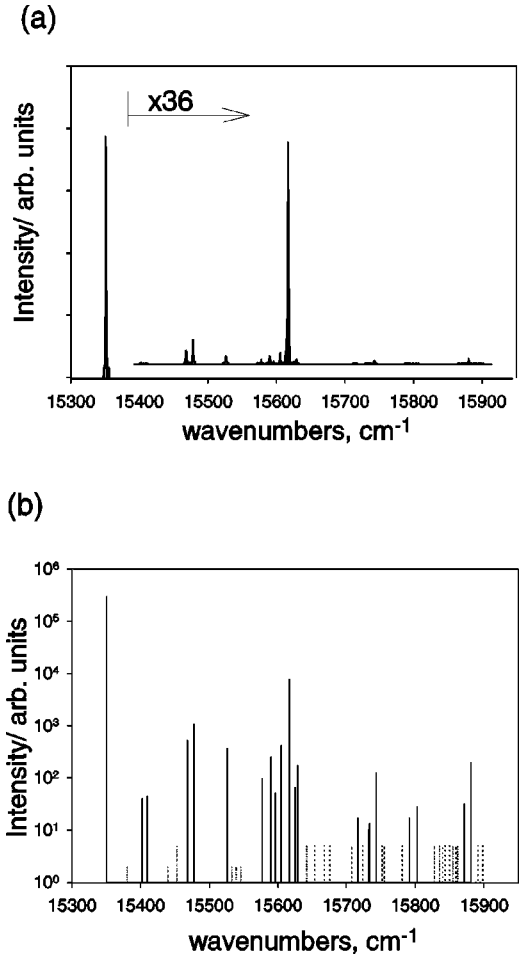

FIG. 3. (a) Electronic $1+1'$REMPI spectrum of $Ca_2{}^{35}Cl_3$ (m/e = 185 amu). All bands beyond the origin are magnified by ×36. (b) Stick spectrum of $Ca_2{}^{35}Cl_3$ plotted on a log scale. Dotted lines indicate weak and very weak bands for which the intensities were not quantified due to saturation.

All bands in the spectra have partially resolved structure, which is dominated by two components split by approximately $0.8 \pm 0.2\ cm^{-1}$. The splitting is consistent throughout the spectrum. It is similar for both $Ca_2{}^{35}Cl_3$ and $Ca_2{}^{35}Cl_2{}^{37}Cl$, and appears to be the same for the $Ca_2{}^{35}Cl{}^{37}Cl_2$ and $Ca_2{}^{37}Cl_3$ bands, as well. Figure 4(a) shows the splitting in the 0–0 band at 15 350.8 cm^{-1} for both $Ca_2{}^{35}Cl_3$ (solid line) and $Ca_2{}^{35}Cl_2{}^{37}Cl$ (dotted line). The overall width is comparable to that expected from the rotational contour of a molecule of this size at 7 K–10 K.

1. Spectrum of $Ca_2{}^{35}Cl_3$

In the spectrum of $Ca_2{}^{35}Cl_3$ we observe 46 weak vibronic bands located from 29 to 632 cm^{-1} to the blue of the origin. The band intensities vary by more than four orders of magnitude. The 21 most intense bands were scanned under unsaturated conditions, but the weaker bands had to be collected at higher laser powers due to lower signal-to-noise ratio.

Table I lists the frequencies and intensities of the bands, as well as frequencies relative to the first band. The frequen-

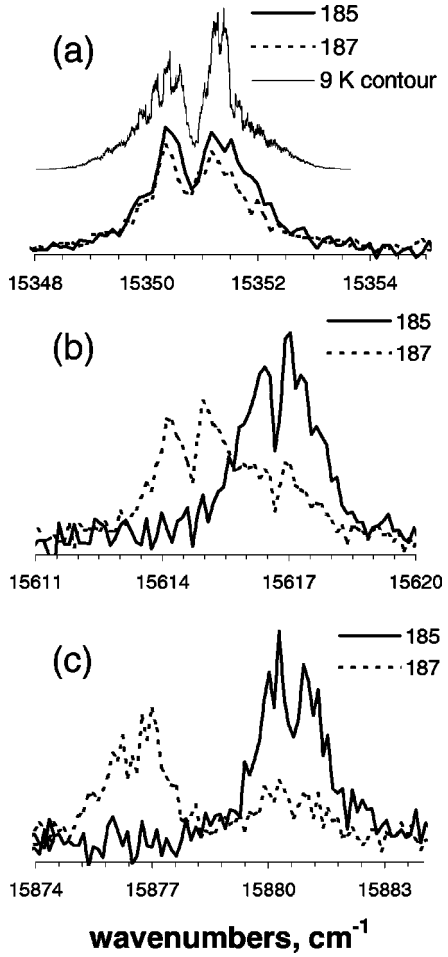

FIG. 4. Overlaid vibronic bands of the isotopomers $Ca_2{}^{35}Cl_3$ (185 amu, solid line) and $Ca_2{}^{35}Cl_2{}^{37}Cl$ (187 amu, dotted line). (a) Origin at 15 350.8 cm^{-1} with a simulation of *b*-type rotational contour at 9 K (offset curve), (b) ν_8 at 15 616.7 cm^{-1}, and (c) $2\nu_8$ at 15 881 cm^{-1}.

cies given are the band centers. The intensities of the weaker bands are listed as weak or very weak; these bands are likely to be saturated.

Figure 3(a) shows the 21 unsaturated bands, with the weaker vibronic bands scaled up by 36 times relative to the strongest band. The dominant band centered at 15 350.8 cm^{-1}, which is furthest to the red, is henceforth assigned as the origin (0–0) band. The second strongest band, at 15 616.7 cm^{-1}, is 40 times smaller than the origin, and the third strongest band, at 15 478.1 cm^{-1}, is 300 times smaller. Many of the weaker bands are barely discernible on a linear scale. All bands are therefore shown in Fig. 3(b) on a semilogarithmic stick spectrum. The weaker bands detected under saturated conditions are shown as dotted lines.

2. Spectrum of $Ca_2{}^{35}Cl_2{}^{37}Cl$

The spectrum of $Ca_2{}^{35}Cl_2{}^{37}Cl$ is nearly identical to that taken for $Ca_2{}^{35}Cl_3$. All the same bands are present. However, the bands exhibit small redshifts as large as 4.4 cm^{-1} relative to the frequencies of the $Ca_2{}^{35}Cl_3$ bands, and some of the bands are split into two components. The band frequencies recorded for $Ca_2{}^{35}Cl_2{}^{37}Cl$, together with intensities, vibrational frequencies, shifts ($\Delta\nu^{187}$) and splittings, are listed in Ref. 32.

Figure 5 shows a portion of the spectra of $Ca_2{}^{35}Cl_3$ (solid line) and $Ca_2{}^{35}Cl_2{}^{37}Cl$ (dotted line) from 15 570 to 15 640 cm^{-1}. These spectra were collected in a single scan, and thus some of the bands are saturated. The shifts and splittings seen here are representative of those observed throughout the spectrum of $Ca_2{}^{35}Cl_2{}^{37}Cl$. The isotope shifts in the region shown in this figure range from 0.0 to 2.1 cm^{-1}. The intensities of the $Ca_2{}^{35}Cl_2{}^{37}Cl$ bands are comparable to those of the $Ca_2{}^{35}Cl_3$ isotopomer bands, with the exception of the $Ca_2{}^{35}Cl_2{}^{37}Cl$ band at 15 623.4 cm^{-1}, which is nine times stronger.

The magnitudes of the redshifts and splittings increase with increasing frequency. This trend can be seen in Fig. 4, where the spectra of $Ca_2{}^{35}Cl_3$ (solid line) and $Ca_2{}^{35}Cl_2{}^{37}Cl$ (dotted line) are overlaid for three bands. The splitting of the origin band is less than 0.1 cm^{-1} at the origin, 2.0 cm^{-1} for the second strongest band at 15 616.7 cm^{-1}, and 4.4 cm^{-1} for the band furthest to the blue at 15 881.0 cm^{-1}.

Ten of the bands observed in the $Ca_2{}^{35}Cl_3$ spectrum are split into two components in the $Ca_2{}^{35}Cl_2{}^{37}Cl$ spectrum. Typically, one of the split components of $Ca_2{}^{35}Cl_2{}^{37}Cl$ is shifted a few wavenumbers to the red, and the other component exhibits little or no shift relative to the $Ca_2{}^{35}Cl_3$ band. In Fig. 5, three of the six bands of $Ca_2{}^{35}Cl_3$ are split into two bands in the $Ca_2{}^{35}Cl_2{}^{37}Cl$ spectrum. The band observed at 15 577.3 cm^{-1} in the $Ca_2{}^{35}Cl_3$ spectrum splits into the bands at 15 575.5 and 15 577.0 cm^{-1} in the $Ca_2{}^{35}Cl_2{}^{37}Cl$ spectrum. Similarly, the band at 15 628.9 cm^{-1} splits into the 15 626.8 and 15 628.3 cm^{-1} bands. For the stronger band in the spectrum at 15 616.7 cm^{-1}, the split is not completely discernable and the nonshifted component appears as a shoulder to the shifted component. Figure 4(b) shows the 15 616.7 cm^{-1} band in closer detail. The intensity of the shifted component is approximately twice as intense as the nonshifted. The addition of the intensity of both components is comparable to that of the single $Ca_2{}^{35}Cl_3$ band.

3. Spectra of $Ca_2{}^{35}Cl{}^{37}Cl_2$ and $Ca_2{}^{37}Cl_3$

The spectra recorded for $Ca_2{}^{35}Cl{}^{37}Cl_2$ and $Ca_2{}^{37}Cl_3$ display the same trends as the spectra of the lighter isotopomers. Due to lower signal to noise, these spectra were taken under saturated conditions. All of the intense bands were observed, but weaker bands were undetected. The redshifts are larger for the heavier isotopomers. The observed bands for $Ca_2{}^{35}Cl{}^{37}Cl_2$ and $Ca_2{}^{37}Cl_3$, along with the vibrational frequencies relative to the origin, and the frequency shifts relative to the $Ca_2{}^{35}Cl_3$ bands are listed in Ref. 32.

The spectrum of $Ca_2{}^{35}Cl{}^{37}Cl_2$ has splittings similar to those of the di-substituted isotopomer, $Ca_2{}^{35}Cl_2{}^{37}Cl$. Three of the stronger peaks at 15 574, 15 613, and 15 739 cm^{-1} have discernible splittings. No splitting of bands is observed in the spectrum of $Ca_2{}^{37}Cl_3$.

TABLE I. Observed vibronic transitions of $Ca_2{}^{35}Cl_3$ ($m/e=185$ amu). ν^{185} are the observed vibrational frequencies with respect to the origin. Bands are assigned to the $^2B_2 \leftarrow \tilde{X}^2A_1$ electronic transition of the C_{2v} planar ring structure. Predicted vibrational frequencies are from B3LYP/6-311+G(3df) calculations. Combination bands are calculated with the observed fundamental vibrational frequencies.

Frequency /cm^{-1}	ν^{185} /cm^{-1}	Relative intensity[a]	Assignment[b]		Calculated frequencies: Fundamental (DFT)/cm^{-1}	Calculated frequencies: Combination bands empirical[b,c]/cm^{-1}
15 350.8	0.0	1000.0	0–0			
15 380.6	29.8	vw	ν_1	B_1	29.9	
15 402.2	51.5	0.1	ν_2	B_2	47.4	
15 409.9	59.1	0.1	$2\nu_1$	A_1		59.6
15 440.0	89.3	vw	ν_3	B_1	88.8	
15 453.2	102.5	w	$2\nu_2$	A_1		102.9
15 468.0	117.3	1.7	$\nu_1+\nu_3,(4\nu_1)$	A_1		119.1, (119.2)
15 478.1	127.4	3.3	ν_4	A_1	123.8	
15 526.0	175.3	1.2	$2\nu_3,(6\nu_1)$	A_1		178.6, (178.8)
15 533.0	182.3	vw				
15 539.0	188.3	vw	$2\nu_1+\nu_4$	A_1		187.0
15 546.0	195.3	vw				
15 577.3	226.5	0.3	ν_6	A_1	230.6	
15 589.7	239.0	0.8	$2\nu_1+2\nu_3,(8\nu_1)$	A_1		238.4, (238.2)
15 596.2	245.5	0.2	ν_7	A_1	247.3	
15 605.1	254.4	1.4	$2\nu_4$	A_1		254.7
15 616.7	266.0	23.4	ν_8	B_2	260.3	
15 625.2	274.5	0.2				
15 628.9	278.2	0.7	$\nu_2+\nu_6$	B_2		278.0
15 640.0	289.3	w				
15 642.0	291.3	w				
15 648.0	297.3	w				
15 653.0	302.3	w				
15 669.0	318.3	w	$\nu_2+\nu_8$	A_1		317.4
15 677.0	326.3	w	$2\nu_1+\nu_8$	B_2		325.6
15 695.0	344.3	w		A_1		
15 704.0	353.3	w		A_1		
15 708.0	357.3	w		A_1		
15 716.6	365.9	0.1	$2\nu_2+\nu_8$	B_2		368.9
15 725.0	374.3	w				
15 732.7	382.0	0.1	ν_9	A_1		381.1
15 733.5	382.8	0.1	$\nu_1+\nu_3+\nu_8,(4\nu_1+\nu_8),(3\nu_4)$	$B_2,(B_2),(A_1)$		385.1, (385.2), (382.2)
15 742.9	392.2	0.4	$\nu_4+\nu_8$	B_2		393.3
15 745.0	394.3	w				
15 791.8	441.0	0.1	$2\nu_3+\nu_8,(6\nu_1+\nu_8)$	B_2		444.6, (444.8)
15 794.0	443.3	w	$\nu_2+\nu_4+\nu_8$	A_1		445.0
15 803.1	452.4	0.1	$2\nu_6$	A_1		453.1
15 828.0	477.3	w				
15 835.0	484.3	w				
15 841.0	490.3	w	$\nu_6+\nu_8,2\nu_7$	B_2,A_1		492.5, 491.8
15 855.0	504.3	w				
15 871.0	520.3	0.1	$2\nu_4+\nu_8$	B_2		520.8
15 881.0	530.3	0.6	$2\nu_8$	A_1		532.0
15 890.0	539.3	w		A_1		
15 899.0	548.3	w				
15 903.0	552.3	w				
15 983.0	632.3	w				

[a]W, weak; vw, very weak. Bands with intensity not quantified due to saturation.
[b]Assignments in parentheses are less likely based on poor agreement with isotopomer shifts.
[c]Combination bands calculated using the experimentally observed fundamental frequencies.

IV. QUANTUM CHEMISTRY CALCULATIONS

A. Density functional theory (DFT) calculations

Ab initio calculations using the GAUSSIAN98[33] software package were performed to aid in assigning the spectra. Geometries were optimized and vibrational frequencies calculated using the B3LYP DFT method and the 6-311+G(3df) basis set. Optimized ground state energies were computed at the MP2(FC)/6-311+G(2df) level. Excited electronic state properties were calculated using the configuration interaction-singles (CIS) method and, where possible, symmetry constrained B3LYP method.

Three stable isomers of Ca_2Cl_3 were found: a C_{2v} planar V-shaped structure (V), a D_{3h} trigonal bipyramid, and a C_{2v} planar ring. The calculated geometries are shown in Fig. 6. The ring is the lowest energy structure of the three. The

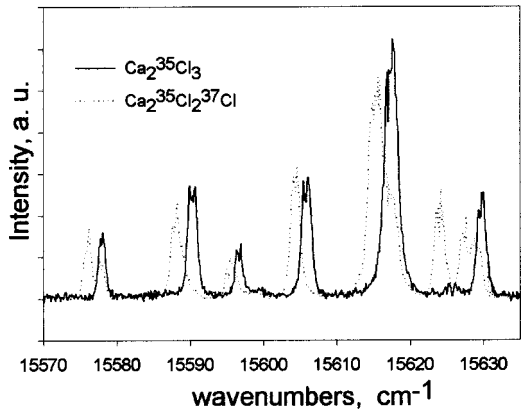

FIG. 5. Comparison of a portion of the spectrum of $Ca_2{}^{35}Cl_3$ (185 amu, solid line) and of $Ca_2{}^{35}Cl_2{}^{37}Cl$ (187 amu, dotted line). These spectra are partially saturated.

bipyramid structure is 34.1 kJ/ mol higher in energy than the ring, and the V structure is 76.7 kJ/mol higher in energy than the ring structure. Vibrational frequencies and excited electronic state calculations were performed for the three structures. Tables II and III list the coordinates, energies, vibrational frequencies, and the excited electronic states for these geometries.

1. Planar C_{2v} V structure

We initially attempted to find a linear isomer, but both $D_{\infty h}$ and $C_{\infty v}$ forms were transition states. Upon lifting all symmetry constraints, the geometry relaxed to the C_{2v} V structure [Fig. 6(a)]. In this planar isomer the Ca atoms in two Ca–Cl moieties are bound to a central, but off-axis chlorine atom, Cl(1), and appear to be slightly bound to each other as well. The Ca–Cl bond lengths are $r1=2.459$ Å in the CaCl(2) subgroups and a somewhat longer $r2=2.661$ Å between the Ca atoms and Cl(1). For comparison, the Ca–Cl distance is 2.437 Å in CaCl,[27] 2.20 Å in $CaCl^+$,[16] and 2.74 Å in the hydrophilite salt structure of $CaCl_2(s)$.[34] The Ca–Ca bond distance is 3.716 Å, which is closer than the 4.277 Å distance in the ground state of the Ca_2 dimer.[35] The identical calcium atoms share equally the unpaired electron. This suggests the formation of a partial σ bond between the Ca atoms.

In this geometry, there are two symmetry distinct chlorine sites, the central Cl(1) atom and the terminal Cl(2) atoms. The $Ca_2{}^{35}Cl_2{}^{37}Cl$ and $Ca_2{}^{35}Cl{}^{37}Cl_2$ isotopomers each have two possible isomers, with C_{2v} and C_s symmetries, depending on which chlorine atoms are substituted.

The nine fundamental vibrational modes for the V structure range from 3.8 to 387.4 cm^{-1}. Five excited electronic states, $^2B_1$, $^2B_2$, $^2A_1$, $^2A_1$, and $^2A_2$, were calculated with the corresponding vertical transitions ranging from 2.18 to 4.55 eV at the CIS level of theory.

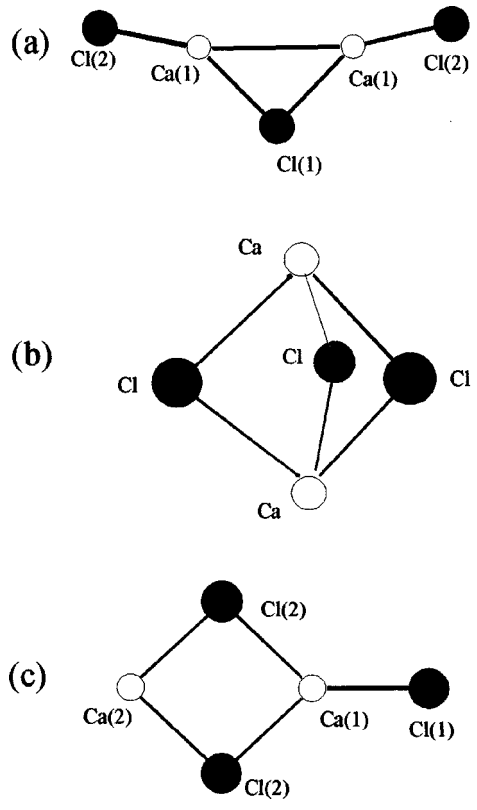

FIG. 6. Structures of Ca_2Cl_3 predicted by B3LYP/6-311G+(3d,f), density functional theory calculations. (a) C_{2v} planar V, (b) D_{3h} trigonal bipyramid, and (c) C_{2v} planar ring.

2. Trigonal bipyramid D_{3h} structure

In the bipyramid structure, the calcium atoms lie above and below the plane of the three chlorine atoms. Each calcium atom bonds to all three chlorine atoms. The Ca–Cl distance ($r1$) is 2.663 Å, while the Cl–Cl distance ($r2$) is 3.593 Å. The distance between the calcium atoms is 3.361 Å, which is closer than in the V structure. The unpaired electron is equally shared between both calcium atoms.

We calculated six vibrational modes, three of which are degenerate, for the ground state of the bipyramid structure with frequencies ranging from 112.7 to 293.5 cm^{-1}. Six excited electronic states were calculated, of which two are degenerate. The $^2A_2''$ state, at 0.04 eV above the ground state, is significantly lower than the other states. Transitions to the higher states (Table III) range from 1.77 to 2.50 eV at the CIS level of theory. Because this isomer has D_{3h} symmetry, Jahn–Teller distortion will occur for the degenerate excited electronic states. In addition, pseudo-Jahn–Teller effects may occur, because all states occur in nearly degenerate pairs of prime and double-prime symmetry, which will be mixed by breaking the symmetry to form a C_{3v} structure.

3. Planar C_{2v} ring structure

The ring structure [Fig. 6(c)] has a four-member ring with two chlorine atoms [Cl(2)] bridging the Ca(1) and Ca(2) atoms. The third chlorine atom, which we denote as the terminal or tail Cl(1), extends from Ca(1) as a tail from the ring. Ca(1) is thus bound to three Cl atoms. The Ca–Cl distances are 2.651 Å($r2$) and 2.666 Å($r3$) in the ring structure and 2.463 Å($r1$) for the tail Ca(1)–Cl(1) bond. The Ca–Ca distance is 3.883 Å.

Unlike the V and the bipyramid isomers, the unpaired electron is localized on just one calcium atom, Ca(2). The

TABLE II. Calculated geometries, energies, and vibrational frequencies of the lowest-lying states of the C_{2v} planar ring $Ca_2{}^{35}Cl_3$ structure. From B3LYP/6-311+G(3df) calculations, unless otherwise noted.

		$\tilde{X}\,{}^2A_1$	$^2B_1$	$^2B_2$	$^2A_1$	$^2A_2$	Experiment
			Coordinates				
$r1$ (Å)	Ca(1)–Cl(1)	2.463	2.463	2.467		2.485	
$r2$ (Å)	Ca(1)–Cl(2)	2.651	2.652	2.644		2.623	
$r3$ (Å)	Ca(2)–Cl(2)	2.666	2.658	2.666		2.731	
α (deg)	Ca(1)–Cl(2)–Ca(2)	93.0	91.5	92.8		92.3	
β (deg)	Cl(2)–Ca(1)–Cl(2)	87.3	88.7	87.7		89.9	
			Electrostatic parameters				
μ (Debye)		4.582	5.016	5.243		10.413	
α[b]		587.379	300.035	569.212		286.257	
			Energetics (adiabatic states)				
E_{el} (hartree)	MP2/6-311+G(2d)	−2733.284 68					
E_{el} (hartree)		−2736.211 24	−2736.159 85	−2736.154 07		−2736.141 51	
E_0 (hartree)		−2736.207 59	−2736.156 56	−2736.150 89		−2736.138 03	
ΔE_0 (eV)	(relative to $\tilde{X}\,{}^2A_1$)	0.00	1.389	1.556		1.893	1.9033[a]
ΔE_{el} (eV)	ClS/6-311+G(d)	0.00	1.925	2.132	2.349		
ΔE_{el} (eV)	ClS/6-311+G(2d)	0.00	1.790	2.042	2.181	3.162	
ΔE_{el} (eV)	ClS/6-311+G(3d,f)	0.00	1.747	2.013	2.142	3.058	
ΔE_0 (eV)	ClS/6-311+G(3d,f)	0.00	1.748	2.014	2.141	3.064	
			Vibrational frequencies				
ν_1 (cm^{-1})	B_1	30.2	18.4	29.9	37.0[c]	30.2	29.8
ν_2 (cm^{-1})	B_2	48.8	48.7	47.4	50.6[c]	51.6	51.5
ν_3 (cm^{-1})	B_1	75.1	86.2	88.8	67.5[c]	92.4	89.3
ν_4 (cm^{-1})	A_1	116.8	114.1	123.8	118.6[c]	114.2	127.4
ν_5 (cm^{-1})	B_2	207.7	220.7	205.0	215.4[c]	151.6	N/Obs
ν_6 (cm^{-1})	A_1	225.6	226.0	230.6	218.6[c]	211.6	226.5
ν_7 (cm^{-1})	A_1	249.3	250.7	247.3	245.3[c]	233.7	245.5
ν_8 (cm^{-1})	B_2	265.3	269.1	260.3	263.6[c]	263.2	266.0
ν_9 (cm^{-1})	A_1	382.1	381.4	381.1	381.3[c]	374.4	381.1

[a]Observed optical transition.
[b]Trace of polarizability tensor ($\alpha_{xx}+\alpha_{yy}+\alpha_{zz}$).
[c]ClS/6-311+G(3df).

Mulliken spin density on this atom at the B3LYP level is 99.7%. Thus, the structure appears to be a classical ionically bound cluster composed of Ca^{+1}, Ca^{+2}, and three Cl^- ions. The chromophore is the Ca^{+1} radical ion.

Fundamental vibrational frequencies range from 29 to 381 cm^{-1} for the ground state C_{2v} ring. Two of the three lowest frequency modes are B_1 out-of-plane bends. Three modes are B_2 out-of-plane bends, and, the remaining modes are A_1 symmetry. The highest frequency mode, ν_9, is the Ca–Cl tail stretch.

There are two distinct chlorine sites, the terminal Cl(1) and the two ring Cl(2) sites. This leads to two isotopomers for both the mono-($Ca_2{}^{35}Cl_2{}^{37}Cl$) and di-substituted ($Ca_2{}^{35}Cl{}^{37}Cl_2$) forms. If both ring chlorine atoms are the same isotope, the structure has C_{2v} symmetry; if they are different, the symmetry is C_s. In both the mono- and di-substituted isotopomers, some of the observed vibronic bands are slightly shifted relative to those of the $Ca_2{}^{35}Cl_3$ isotopomer. For some modes, both isomers have the same redshift. For specific modes where either the tail or the ring chlorines dominate the vibration, the C_{2v} and C_s isomers have different redshifts. For example, the ν_9 mode is predominantly the stretch of the terminal Ca–Cl bond. In the C_{2v} isomer of $Ca_2{}^{35}Cl_2{}^{37}Cl$, the ^{37}Cl is substituted at the tail, and the frequency is shifted; in the C_s structure, the frequency has almost no shift since the tail Cl is a ^{35}Cl atom.

Four excited electronic states—$^2B_1$, $^2B_2$, $^2A_1$, and $^2A_2$—were calculated at the CIS level for the ring structure and found to have adiabatic transition energies ranging from 1.75 to 3.06 eV (see Table II). Oscillator strengths are 0.2174, 0.1739, 0.1400, and 0.000, respectively. Excitation to the $^2A_2$ state is dipole forbidden.

B. Excited electronic states of the planar C_{2v} ring isomer

Close agreement between the experimental data and the calculated properties of the C_{2v} ring structure (see analysis section below) warranted further calculations for this structure. The coordinates, excitation energies, and vibrational frequencies were calculated for three of the excited electronic states $^2B_1$, $^2B_2$, and $^2A_1$ (see Table II).

Two methods were used to calculate the excited electronic state energies of the C_{2v} ring structure. Table II shows the B3LYP and CIS excited state energies. CIS results are listed for three augmented basis sets, 6-311+G(d), 6-311+G(2d), and 6-311+G(3d,f). The results do not converge, but the differences between states diminish with increasing basis sets. The B3LYP energies are significantly lower than the CIS energies.

TABLE III. Calculated properties of two higher energy isomers of Ca_2Cl_3. See Fig. 6 for atom definition. From B3LYP/6-311+G(3d,f) calculations, unless otherwise noted.

C_{2v} planar V structure			D_{3h} trigonal bipyramid structure		
		Coordinates			
		$\tilde{X}\,^2A_1$			$\tilde{X}^2A_1'$
$r1$ (Å)	Ca(1)–Cl(1)	2.454	$r1$ (Å)	Ca–Cl	2.663
$r2$ (Å)	Ca(1)–Cl(2)	2.655	$r2$ (Å)	Cl–Cl	3.593
α (deg)	Ca(1)–Cl(2)–Ca(1)	89.0	α (deg)	Ca–Cl–Ca	84.9
β (deg)	Cl(1)–Ca(1)–Cl(2)	144.8	β (deg)	Ca–Cl–Ca	77.6
		Energetics			
E_{el} (hartree)	MP2/6-311+G(2d)	−2733.255 45			−2733.271 69
ΔE_{el} (kJ/mol)	Relative to E_{el} (ring)	76.695			34.065
E_{el} (hartree)	B3LYP/6-311+G(2d)	−2736.180 22			−2736.195 26
E_0 (hartree)	B3LYP/6-311+G(2d)	−2736.177 00			−2736.191 49
ΔE_0 (kJ/mol)	Relative to E_0 (ring)	58.690			20.647
		Vibrational frequencies			
ν_1 (cm^{-1})	B_1	3.8	ν_1 (cm^{-1})	E'	112.7
ν_2 (cm^{-1})	A_2	27.0	ν_2 (cm^{-1})	A_2''	131.6
ν_3 (cm^{-1})	A_1	35.7	ν_3 (cm^{-1})	E''	169.0
ν_4 (cm^{-1})	B_2	55.6	ν_4 (cm^{-1})	A_A'	169.2
ν_5 (cm^{-1})	A_1	96.0	ν_5 (cm^{-1})	E'	260.5
ν_6 (cm^{-1})	B_2	207.8	ν_6 (cm^{-1})	A_1'	293.5
ν_7 (cm^{-1})	A_1	244.0			
ν_8 (cm^{-1})	B_2	366.3			
ν_9 (cm^{-1})	A_1	387.4			
		Excited electronic states ClS/6-311+G(3df) (vertical transitions)			
State	ΔE_{el} (eV)	Oscillator strength	State	ΔE_{el} (eV)	Oscillator strength
$^2B_1$	2.1815	0.1735	$^2A_2''$	0.040	0.0291
$^2B_2$	2.8026	0.2698	$^2E'$	1.775	0.2336
$^2A_1$	3.1789	0.0027	$^2E''$	1.834	0.0000
$^2A_1$	3.5842	0.1837	$^2A_1'$	2.2642	0.0000
$^2A_2$	4.5466	0.0000	$^2A_1'$	2.4432	0.0000
			$^2A_2''$	2.505	0.0748

Geometries and frequencies for the $^2B_1$, $^2B_2$, and $^2A_2$ states were calculated with the B3LYP method and the 6-311+G(3df) basis set. CIS calculations were used for the $^2A_1$ state. Overall, the geometries of the four excited electronic states and the ground state are very similar. Angles and bond lengths vary by less than 3%. Variations in the vibrational frequencies among the states are highest in the ν_1, ν_3, and ν_5 calculated modes, but are less than 10% in the other six modes.

V. ASSIGNMENT OF SPECTRA

A. Isomeric assignment

The observed pattern of a strong origin, and much weaker vibronic bands indicates that there is little change in the geometry and vibrational frequencies between the ground and excited electronic states. There are no extended vibronic progressions in the spectrum, making the assignment less straightforward. We therefore compare the observed spectrum with predictions for the three different minimum energy structures computed by the DFT method.

1. Planar C_{2v} V structure

The V structure is calculated to be about 76.7 kJ/mol higher than the lowest energy isomer, the ring structure, at the MP2/6-311+G(2d) level. If this isomer is present, it is metastable. At the DFT level, the vertical excitation energies of the two lowest excited electronic states, the $^2B_1$ and $^2B_2$ states, are near the observed transition, although at the CIS level the transition to the $^2B_2$ state is 0.9 eV higher. All other states are much higher in energy and therefore unlikely candidates. However, adiabatic energies for the transitions to the $^2B_1$ and $^2B_2$ are significantly lower than the vertical energies, indicating large geometry changes upon excitation. The electronic spectrum should therefore have a broad Franck–Condon envelope, contrary to observations. The predicted frequencies of the ground state fundamental modes ν_2, ν_4, ν_5, ν_7, and ν_9 are in good agreement with some of the observed bands ($\sigma=4\%$). However, the three strongest observed vibronic bands, at 127.4, 226.5, and 266.0 cm^{-1}, cannot be assigned. The observations are therefore not consistent with assignment to the C_{2v} V structure.

2. Trigonal bipyramid D_{3h} structure

The bipyramid structure is also predicted to be metastable, with energy 34.1 kJ/mol above the lowest energy isomer at the MP2(FC)/6-311+G(2d) level. Six excited electronic states were calculated for the D_{3h} structure. While transitions to two $^2A_2''$ states and a $^2E'$ state are dipole allowed in D_{3h} symmetry, Jahn–Teller and pseudo-Jahn–Teller distortions will lower the symmetry and render all six

transitions allowed. Transitions to the $^2E'$ and $^2E''$ are predicted to be near the observed transition. However, the lowest predicted vibrational frequency for the ground state is 112.7 cm^{-1}; in contrast, the five lowest vibrational bands are observed below 110 cm^{-1}. While nonadiabatic interactions can lead to additional low frequency modes and splittings, the resulting geometric distortions should also lead to substantial intensity in higher vibronic bands. The spectrum does not exhibit the complexity one would expect for this structure.

3. Planar C_{2v} ring structure

The ring structure is the minimum energy isomer calculated. The four lowest electronically excited states, $^2B_1$, $^2B_2$, $^2A_1$, and $^2A_2$, all lie within 0.5 eV of the observed transition at both B3LYP and CIS/6-311+G(3df) levels of theory. All of the excited electronic states are predicted to have nearly the same geometry and vibrational frequencies as the ground state. Thus, of the three geometries, only the C_{2v} ring is qualitatively consistent with the observed intensity pattern.

This conclusion is quantitatively borne out in Franck–Condon simulations for three of the transitions, $^2B_1 \leftarrow \tilde{X}\,^2A_1$, $^2B_2 \leftarrow \tilde{X}\,^2A_1$, and $^2A_2 \leftarrow \tilde{X}\,^2A_2$. Simulations were performed using the B3LYP optimized geometries and frequencies. For each of the transitions, the origin band was predicted to be the dominant feature, and the next three strongest bands were the A_1 bands ν_4, ν_7, and ν_9, at 123.8, 230.6, and 381.1 cm^{-1}, respectively. The intensity ratios relative to the origin band were calculated to be 1:0.196:0.017:0.001, 1:0.004:0.002:0.004, and 1:0.023:0.105:0.071, for the transitions to the $^2B_1$, $^2B_2$, and $^2A_2$ states, respectively. The experimental ratio of the strongest of the allowed bands, the ν_4 mode, to the origin band is 1:0.003. Thus, the Franck–Condon factors for the ring structure are consistent with the observed spectrum, with the transition to the $^2B_2$ state giving very good agreement.

There are many more bands in the observed spectrum than are predicted by the Franck–Condon simulation. However, the vibronic bands are extremely weak (two to four orders of magnitude less than the origin). Thus, one might expect additional bands that arise from higher order effects resulting from breakdown of the double-harmonic approximation, e.g., Franck–Condon forbidden transitions which gain intensity from anharmonicity, large-amplitude motion, coordinate dependence of the dipole moment, or vibronic coupling.

A comparison of the predicted and observed vibrational frequencies provides an additional test of the structural assignment. The calculated vibrational frequencies of all excited electronic states are nearly identical with those of the ground state (see Table II). Predicted frequencies for eight of the nine fundamental modes (all but ν_5) are in very good agreement with bands observed in the $Ca_2{}^{35}Cl_3$ spectrum. The average RMS error is 6.9% between observed frequencies and the average of the calculated frequencies (average of the $\tilde{X}\,^2A_1$, $^2B_1$, $^2B_2$, and $^2A_2$ frequencies computed at the B3LYP level).

Of the three isomers, the C_{2v} ring is therefore the only structure whose spectral properties are consistent with the observed spectrum. Furthermore, the excellent agreement between the predicted and observed vibrational frequencies provides strong quantitative support for this assignment.

B. Assignment of the excited electronic state

All four of the predicted excited electronic states of the ring isomer have similar vibrational frequencies and geometries, and are thus qualitatively consistent with the observed spectrum. However, we have seen that the observed intensity pattern and the vibrational frequencies are most consistent with assignment to the $^2B_2 \leftarrow \tilde{X}\,^2A_1$ transition. The Franck–Condon simulation of this transition gives the best agreement with the observed intensities of the few A_1 vibronic bands relative to the origin. Furthermore, the vibrational frequencies of the $^2B_2$ state at the B3LYP level are closest to the observed frequencies, with a standard deviation of 3%, while the $\tilde{X}\,^2A_1$, $^2B_1$, and $^2A_2$ have deviations of 6%, 13%, and 4%, respectively. However, this analysis excludes consideration of the excited $^2A_1$ state, for which we cannot perform geometry optimized B3LYP calculations.

The symmetry of the excited electronic state can be determined unambiguously from the rotational structure. We have simulated the rotational band contours of the origin expected for the $^2B_1 \leftarrow \tilde{X}\,^2A_1$, $^2B_2 \leftarrow \tilde{X}\,^2A_1$, and $^2A_1 \leftarrow \tilde{X}\,^2A_1$ transitions. The calculations were done in the rigid rotor approximation, using the B3LYP rotational constants and neglecting spin–rotation fine structure. The contour for the $^2B_2 \leftarrow \tilde{X}\,^2A_1$ transition, shown in Fig. 4(a), matches the 15 350.8 cm^{-1} band shape well. This is a *b*-type transition, which has a gap at the origin. In contrast, the $^2A_1 \leftarrow \tilde{X}\,^2A_1$ transition is an *a*-type transition which would have a large central *Q* branch. Excitation to the $^2B_1$ state will give rise to a *c*-type transition, which also possesses strong *Q* branches. Finally, we can rule out the $^2A_2$ state, because transitions to this state are dipole forbidden. Furthermore, there are no vibrational modes of A_2 symmetry, so there is no first order mechanism for a vibronically allowed transition. Thus, from the partially resolved rotational structure we assign this spectrum to the $^2B_2 \leftarrow \tilde{X}\,^2A_1$ transition.

C. Assignment of the vibronic bands

1. Vibronic bands of $Ca_2{}^{35}Cl_3$

There were 47 bands observed in the spectrum of $Ca_2{}^{35}Cl_3$. Of these, the 20 most intense and another eight of the weaker features were assigned to fundamental, overtones, and combination bands of the transitions to the $^2B_2$ excited electronic state of the C_{2v} ring structure. The band assignments, including symmetry and calculated frequencies, are included in Table I. In this table, the predicted vibrational frequencies of the overtone and combination bands are calculated from the observed fundamental frequencies. Multiple assignments are listed where more than one is possible, and the less likely assignments are given in parentheses.

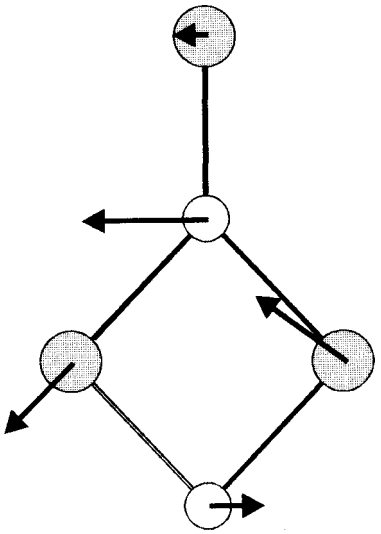

FIG. 7. Displacement for the ν_8 normal mode of the C_{2v} planar ring structure. Arrows show relative displacements, but are not to scale.

The calculated fundamental modes have three symmetries, A_1, B_1, or B_2, as listed in Table II. All modes except ν_5 have been assigned to bands in the spectra. The A_1 symmetry modes observed are ν_4, ν_6, ν_7, and ν_9. The ν_4 band is the third most intense in the spectrum and about 300 times weaker than the origin. The other three are all of similar intensity, approximately 5000 times weaker than the origin. The B_2 symmetry modes observed are ν_2 and ν_8. The ν_8 band (see Fig. 7) is the strongest vibronic band after the origin and is about 40 times weaker than the origin. The ν_2 band is approximately 5000 times weaker than the origin. Two B_1 symmetry bands are observed, ν_1 and ν_3. These bands were just slightly above noise level, even at the highest laser powers, and were therefore several orders of magnitude weaker than the other observed bands.

The other 20 bands we assign comprise overtones and combinations. The frequencies of the overtones and combination bands were computed empirically from the observed fundamental mode frequencies. All assigned combination bands agree to within 5 cm^{-1} with the observed band frequencies. Seven of the bands can be assigned to more than one possible combination. Five of these seven are due to the accidental resonance $3\nu_1 \sim \nu_3$, which is propagated into overtones and combinations such as $4\nu_1 \sim \nu_1 + \nu_3$ and $6\nu_1 \sim 2\nu_3$.

Of the 10 bands observed above 15 650 cm^{-1}, eight arise from the combinations of ν_8 with other fundamental modes including its overtone, $2\nu_8$. These combination bands have B_2 symmetry, with the exception of combinations with ν_2 and the overtone $2\nu_8$, which are A_1 symmetry. There are therefore from nine to eleven bands of B_2 symmetry observed in the spectrum.

The B_2 modes are not Franck–Condon allowed, yet their intensities are comparable to the Franck–Condon allowed A_1 bands. The B_2 band ν_8 is the second most intense peak after the origin. This suggests that the excited electronic may have B_2 symmetry, as the B_2 vibrations would then become vibronically allowed by Herzberg–Teller coupling.

2. Vibronic bands of $Ca_2{}^{35}Cl_2{}^{37}Cl$ (187 amu)

The spectra of $Ca_2{}^{35}Cl_3$ and $Ca_2{}^{35}Cl_2{}^{37}Cl$ are nearly identical, except for the presence of small redshifts and splittings of some of the bands. The shifts are small near the origin, $\leqslant 0.1$ cm^{-1}, and increase to 4.4 cm^{-1} at the highest frequency band. We were able to assign 37 of the 50 observed bands of $Ca_2{}^{35}Cl_2{}^{37}Cl$ on the basis of our assignment of the $Ca_2{}^{35}Cl_3$ spectrum. Components of split peaks were assigned to the two possible isomers of $Ca_2{}^{35}Cl_2{}^{37}Cl$, which have C_s and C_{2v} symmetry. The observed bands, the isotopic shifts, and their assignments are listed in Ref. 32.

The calculated and observed isotopic frequency shifts of $Ca_2{}^{35}Cl_2{}^{37}Cl$ are in good agreement. Where splittings are observed, we assign the split components based on the predicted frequency shifts of the C_s and C_{2v} isomers and the relative intensity of the components. The intensity ratio of the C_s to C_{2v} components is nearly 2:1. Both the shifts and relative intensities are consistent. In the cases where the isomers were unresolved, we have calculated average properties of both isomers.

The isotopic shifts often help to resolve ambiguities where two or more assignments in the $Ca_2{}^{35}Cl_3$ spectrum are possible. For example, the band at 15 524.8 cm^{-1}, which can be assigned to either $\nu_1 + \nu_3$ or $6\nu_1$, has a red shift of 1.2 cm^{-1}. The predicted redshift for $\nu_1 + \nu_3$ is 0.8 cm^{-1}, while that for $6\nu_1$ is 0.3 cm^{-1}, favoring the $\nu_1 + \nu_3$ assignment. The same is true for all bands where the accidental resonance $3\nu_1 \sim \nu_3$ leads to two possible assignments. In all cases, $\nu_1 + \nu_3$ or ν_3 progressions are in better agreement with the observed shifts than are the even overtones of ν_1.

3. Vibronic bands of $Ca_2{}^{35}Cl{}^{37}Cl_2$ (189 amu) and $Ca_2{}^{37}Cl_3$ (191 amu)

The assignments of the $Ca_2{}^{35}Cl{}^{37}Cl_2$ and $Ca_2{}^{37}Cl_3$ bands are similar to those of $Ca_2{}^{35}Cl_2{}^{37}Cl$ and $Ca_2{}^{35}Cl_3$, respectively. The bands of both isotopomers are redshifted, and the shifts are largest for the heaviest isotopomer, $Ca_2{}^{37}Cl_3$. In three of the bands of $Ca_2{}^{35}Cl{}^{37}Cl_2$, isotopic splittings are observed. No splitting is observed in the $Ca_2{}^{37}Cl_3$ spectrum. The bands observed for $Ca_2{}^{35}Cl{}^{37}Cl_2$ and $Ca_2{}^{37}Cl_3$ are listed in Ref. 32.

VI. DISCUSSION

Ca_2Cl_3 has a strong electronic transition at 15 350.8 cm^{-1} (651.2 nm) and several weak but sharp vibronic bands with partially resolved rotational contours. Of the three minimum energy isomers found in the DFT calculations, a C_{2v} planar ring form is the only structure that qualitatively and quantitatively agrees with the observed spectrum. We have assigned this spectrum to a $^2B_2 \leftarrow \tilde{X}\,^2A_1$ electronic transition of Ca_2Cl_3 of the planar C_{2v} ring geometry. The geometry and frequencies of this isomer are predicted to remain unchanged upon excitation to electronic states accessible in this spectral region. This prediction is in agreement with the prominent origin band in the observed spectrum, which is $\sim$40 times more intense than the second strongest band. Franck–Condon simulations reproduce the intensity pattern, with excellent agreement for the $^2B_2 \leftarrow \tilde{X}\,^2A_1$ transition. In

contrast, DFT calculations predict large changes upon excitation to the lowest states of the other isomers, the C_{2v}V structure and the D_{3h} trigonal bipyramid. The partially resolved rotational contour matches well with a simulated *b*-type (B_2) transition of the ring structure, consistent with a $^2B_2 \leftarrow {}^2A_1$ electronic transition. The observed vibronic band spacings are in good agreement with the vibrational frequencies calculated for the ring structure, with the $^2B_2$ state giving the best fit.

The ν_8 band at 15 616.7 cm^{-1} has a special role in this transition. It is the second strongest feature in the spectrum, despite the fact that it is not Franck–Condon allowed. Although the band is 40 times less intense than the origin, it is an order of magnitude larger than the next strongest vibronic band (a Franck–Condon allowed A_1 mode). Furthermore, most of the bands above 15 650 cm^{-1} are combinations of the ν_8 band with lower frequency vibronic bands originating from the 0–0 band. The main spectral pattern is essentially repeated twice (the intensity pattern is qualitatively similar), with the much weaker sequence above 15 650 cm^{-1} originating at the ν_8 band.

Almost all of the Franck–Condon forbidden bands, including the ν_8 band and most of the subsequent combination bands, are of B_2 symmetry. These bands most likely gain intensity through the dependence of the transition dipole moment operator on the Q_8 normal mode, which can be estimated from the first term in a Taylor series expansion:

$$\begin{aligned}\langle B_2, \nu_8' | \mu(Q_8) | XA_1, \nu'' = 0 \rangle \\ \approx \langle B_2 | \mu_{e1,0} | XA_1 \rangle \langle \nu_8' | X \nu'' = 0 \rangle \\ + \langle B_2 | \partial\mu/\partial Q_8 | A_1 \rangle \langle \nu_8' | Q_8 | A_1, \nu'' = 0 \rangle. \end{aligned} \quad (1)$$

The first term on the right-hand side is the standard Franck–Condon approximation. The second term is the integral of the derivative of the electronic dipole moment operator over the electronic wave functions, times an integral of the normal coordinate Q_8 over the upper and lower vibrational wave functions. For $\nu_8' = 1$, the first term is zero. Calculation of the second term using a numerical derivative of μ at the CIS level and harmonic oscillator approximation for the vibrational factor however leads to a band strength relative to the origin that is several orders of magnitude too small, suggesting that this term needs to be computed explicitly.

We have modeled the structure seen in each band as partially resolved rotational band contours; however the molecule is a doublet, and spin–orbit or spin–rotation effects should also give rise to fine structure. Spin–orbit coupling should be small, as this is a nonplanar molecule for which the spin–rotation coupling is effectively the residual spin–orbit interaction.[23] Bernath and co-workers at Waterloo have observed spin–rotation splittings of >1 cm^{-1} in CaX (X=ligand) molecules. The pure precession model for the spin–rotation parameters in doublet CaX molecules gives[20,22]

$$\varepsilon_{aa} \approx \frac{4\Lambda^2 A A_{so}}{E(^2B_1) - E(^2B_2)}. \quad (2)$$

We can estimate the magnitude of the spin–rotation interaction, if we assume a $B_2 - B_1$ splitting of 1300 cm^{-1} (the minimum consistent with our data) and the free Ca^+ ion spin–orbit coupling of 158 cm^{-1}. In this case, we find that $\varepsilon_{aa} \approx -0.03\ cm^{-1}$, much less than the splitting of the bands or the resolution of the experiment. The larger splittings seen in the systems (such as $CaNH_2$) studied by Whitham and Jungen and by Bernath and co-workers result from the large *A* rotational constants. Thus, the observed ''splitting'' of ≈ 1 cm^{-1} in Ca_2Cl_3 is not spin–rotation fine structure, although fine structure effects may alter the predicted shapes of the rotational band contours.

The DFT calculations predict that 99.7% of the electron spin density resides on the Ca(2) atom, which possesses a charge of almost +1. Ca_2Cl_3 can thus be thought of as an ionic salt cluster of the form:

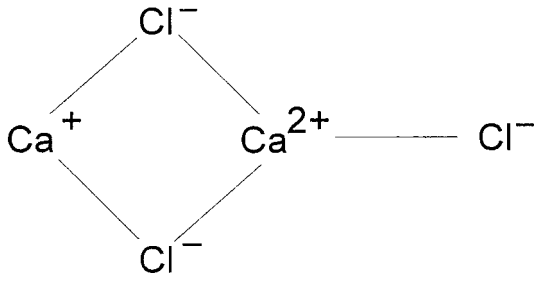

Alternatively, Ca_2Cl_3 can be considered as a Ca^+ ion bound to a $CaCl_3^-$ moiety. The stabilization of this structure originates in the stability of the $CaCl_3^-$, which in turn arises from the strong attraction between the doubly charged calcium cation and the three chloride anions. The lack of any geometry change upon excitation of the Ca^+ electron indicates that the unpaired electron does not participate in any valence bonding; hence, the bonding is entirely ionic.

Localization of the unpaired electron on Ca(2) suggests that the electronic states of Ca_2Cl_3 are those of the Ca^+ ion mixed and shifted in the field of the remaining ions. A population analysis of the orbital composition of the ground and $^2B_2$ states shows that the transition is from a largely $Ca^+ 4s$-like ground state (57% $4s$, 19% $4p$, 11% $3s$, and other) to a mostly Ca^+ $4p$-character $^2B_2$ state (45% $4p$, 28% $5p$, and some contribution from Cl $4p$ and $5s$ orbitals).

Our results suggest that the Ca_2Cl_3 cluster and its low-lying excited states can be treated with a semiempirical one-electron model. One approach is to extend the ligand-field theory developed by Field and co-workers for diatomic alkaline-earth halides. The model Hamiltonian starts with free Ca^+ ion states as the zeroth order basis set and introduces a polarizable closed-shell spherical anion in cylindrical symmetry. Such a model is well suited for the ring structure, which contains the Ca^+ ion, if the polyatomic $CaCl_3^-$ ligand is treated correctly. More generally, a pseudo-potential hamiltonian could be used to describe a single electron moving in the field produced by two Ca^{2+} atomic ions and three Cl^- ions; such a model should be capable of treating all structural isomers of Ca_2Cl_3.

We can contrast Ca_2Cl_3, an alkaline-earth halide radical cluster, to the alkali halide cluster series M_nX_{n-1}, which

also possess an excess electron. In Na_3F_2 for instance, Sence and co-workers[11,13] have shown that the unpaired electron occupies a diffuse orbital. The electron is not tightly bound to a single metal atom, but is in a diffuse orbital around a tail Na^+ atom or a vacancy on an F^- atom. The broad features seen in the Na_3F_2 spectrum contrast with the sharp lines observed in Ca_2Cl_3, where the electron is tightly bound to the Ca(2) atom. Excitation of the diffuse electron in Na_3F_2 is predicted to lead to large changes in the charge distribution and hence large geometry changes; thus, the overall Franck–Condon envelope is predicted to be broad and the vibronic spectra should be congested. In addition, spectra with varying degrees of broadening have been reported for Na_2F;[15] the differences have been attributed to temperature effects. In general, little spectroscopic detail has been resolved.

The electronic structures of the V and bipyramid isomers differ from the ring isomer. In the ring form, the unpaired electron is localized on the Ca(2) atom, but in the higher energy V and bipyramid isomers, the Ca atoms are equivalent and share the unpaired electron. There is significant Ca–Ca bonding in the V isomer, which deviates significantly from linearity due to attraction between the Ca atoms. In the D_{3h} structure, the 0.04 eV splitting between the ground $^2A_1'$ state and the low-lying $^2A_2''$ state ($4s\sigma$ and σ^* bonding orbitals, respectively) is a direct measure of the bonding interaction between the Ca atoms, though this may be mediated by the bridging chlorine atoms. Both isomers are predicted to be metastable minima, but their energies are close to that of the ring structure, and higher level calculations are needed to confirm the relative energetics. These isomers may be formed in the nonequilibrium conditions of a supersonic jet, even if they are metastable. The CIS and DFT calculations predict that these isomers have electronic transitions in the visible or UV that lead to significant changes in cluster geometry. These spectra are expected to have strong Franck–Condon progressions.

The planar C_{2v} ring and D_{3h} bridged structures of Ca_2Cl_3, which are nearly the same energy, are analogous to geometries found by Levy and Hargittai for Ca_2Cl_4 from B3LYP/cc-pVTZ calculations.[6] They find that the lowest energy form of Ca_2Cl_4 is a doubly bridged (D_{2h}) structure with a planar four-member ring and two Cl^- tail atoms. A triply bridged (C_{3v}) isomer, similar to the D_{3h} structure presented in this work but with the additional Cl atom in a Ca–Cl tail bond, lies only 10 kJ/mol higher. Thus, smaller alkaline-earth clusters appear to have multiple low-lying isomers, with similar structural motifs, with competition among geometries with multiple bridging halides. Unlike the M_2X_4 dimers, however, open-shell clusters such as Ca_2Cl_3 possess electronic spectra. Since metastable isomers are readily formed and trapped in supersonic beams, the spectroscopy of radical alkaline-earth halide clusters may allow us to examine bonding and structures of various isomers of Ca_2Cl_3 and larger radical clusters.

The current work opens up many new possible directions in the spectroscopy of alkaline-earth halides. Higher level calculations of the potential energy surfaces of Ca_2Cl_3 are underway to obtain more accurate energetics and to identify reaction pathways for isomerization. Our Ca_2Cl_3 spectra have laser-limited resolution, and it may be fruitful to scan these bands at higher resolution. Finally, our results suggest that one can investigate larger Ca_nCl_{2n-1} clusters, as well as compounds with substitution of the halides and/or alkaline-earth metals.

VII. CONCLUSION

Spectra of the four Ca_2Cl_3 isotopomers were observed in the visible region from 15 350 to 16 000 cm^{-1}. With the aid of DFT calculations, we assigned the spectra to the $^2B_2 \leftarrow \tilde{X}\,^2A_1$ transition of Ca_2Cl_3 in a C_{2v} ring geometry, in which the two Ca atoms are bridged by two chlorine atoms. The predicted intensity pattern, the vibrational frequencies, and the rotational band contour were in very good agreement with the data. The chromophore was found to be the Ca^+ ion.

Our results suggest that the alkaline-earth halide excess-electron clusters may possess sharp, vibrationally and rotationally resolved electronic transitions. Thus, unlike closed shell alkaline-earth halides such as $CaCl_2$ or Ca_2Cl_4 or excess-electron alkali halide clusters, the electronic spectra can provide detailed structural information of these salt clusters and may also serve as a rigorous test of semiempirical models. Such spectra would allow us to address questions concerning the importance of multiple bridging halides, the role of delocalization and metal–metal bonding, and the influence of nonadiabatic effects, e.g., Jahn–Teller distortion.

ACKNOWLEDGMENTS

We acknowledge support of NSF Grant No. CHE9700-610. Funding from the JPL Institutional Computing and Information Services and the NASA Offices of Space Science and Earth Science provided the supercomputer used for some of the calculations. We thank V.-A. Glezakou and P. Bernath for helpful comments.

[1] T. P. Martin, Phys. Rep. **95**, 167 (1983).
[2] J. Lima-de-Faria, *Structural Mineralogy: An Introduction* (Dordrecht, Boston, 1994), 87 pp.
[3] M. Kaupp, P. v. R. Schleyer, H. Stoll, and H. Preuss, J. Am. Chem. Soc. **113**, 6012 (1991).
[4] L. Wharton, R. A. Berg, and W. J. Klemperer, J. Chem. Phys. **39**, 2023 (1963).
[5] A. Buchler, J. L. Stauffer, and W. J. Klemperer, J. Am. Chem. Soc. **86**, 4544 (1964).
[6] J. B. Levy and M. Hargittai, J. Phys. Chem. A **104**, 1950 (2000).
[7] M. Hargittai, Chem. Rev. **100**, 2233 (2000).
[8] T. C. Devore and J. L. Gole, Chem. Phys. **241**, 221 (1999).
[9] U. Landman, D. Scharf, and J. Jortner, Phys. Rev. Lett. **54**, 1860 (1985).
[10] E. C. Honea, P. Labastie, M. L. Homer, and R. L. Whetten, Phys. Rev. Lett. **64**, 2933 (1989).
[11] G. Durand, F. Spiegelmann, Ph. Poncharal, P. Labastie, J.-M. L'Hermite, and M. Sence, J. Chem. Phys. **110**, 7884 (1999).
[12] G. Rajagopal, R. N. Barnett, A. Nitzan, U. Landman, E. C. Honea, P. Labastie, M. L. Homer, and R. L. Whetten, Phys. Rev. Lett. **64**, 2933 (1990).
[13] P. Labastie, J.-M. L'Hermite, Ph. Poncharal, and M. Sence, J. Chem. Phys. **103**, 6362 (1995).
[14] T. Sugai and H. Shinohara, Chem. Phys. Lett. **281**, 57 (1997).
[15] D. T. Vituccio, R. F. W. Herrmann, O. Golonzka, and W. E. Ernst, J. Chem. Phys. **106**, 3865 (1997).
[16] S. F. Rice, H. Martin, and R. W. Field, J. Chem. Phys. **82**, 5023 (1985).
[17] N. A. Harris and R. W. Field, J. Chem. Phys. **98**, 2642 (1993).

[18] R. W. Field and C. M. Gittins, J. Chem. Phys. **106**, 10379 (1997).
[19] N. Honjou, G. F. Adams, and D. R. Yarkony, J. Chem. Phys. **79**, 4376 (1983).
[20] C. J. Whitham and Ch. Jungen, J. Chem. Phys. **93**, 1001 (1990).
[21] Z. Morbi, C. Zhao, and P. F. Bernath, J. Chem. Phys. **106**, 4860 (1997).
[22] Z. Morbi, C. Zhao, J. W. Hepburn, and P. F. Bernath, J. Chem. Phys. **108**, 8891 (1998).
[23] C. N. Jarman and P. F. Bernath, J. Chem. Phys. **98**, 6697 (1993).
[24] E. S. Rittner, J. Chem. Phys. **19**, 1030 (1951).
[25] D. L. Hildenbrand, J. Chem. Phys. **48**, 1657 (1968).
[26] T. Törring, W. E. Ernst, and J. Kändler, J. Chem. Phys. **90**, 4927 (1989).
[27] S. L. Davis, J. Chem. Phys. **89**, 1656 (1988).
[28] L. Klynning and H. Martin, Phys. Scr. **24**, 33 (1981).
[29] S. Raouafi, G. H. Jeung, and C. Jungen, J. Mol. Spectrosc. **196**, 248 (1999).
[30] K. P. Huber and G. Herzberg, *Constants of Diatomic Molecules* (Van Nostrand, New York, 1979), pp. 116–125.
[31] J. M. Spotts, Ph.D. thesis, California Institute of Technology, 1999.
[32] See EPAPS Document No. E-JCPSA6-114-001114 for observed vibronic transitions. This document may be retrieved via the EPAPS homepage (http://www.aip.org/pubservs/epaps.html) or from ftp.aip.org in the directory/epaps/. See the EPAPS homepage for more information.
[33] M. J. Frisch, G. W. Trucks, H. B. Schlegel *et al.*, GAUSSIAN 98, Revision A.5, Gaussian, Inc., Pittsburgh, PA, 1998.
[34] K. Sahl, Acta Crystallogr. **19**, 1027 (1965).
[35] W. J. Balfour and R. F. Whitlock, Can. J. Phys. **53**, 472 (1975).